RCF (Rolling Contact Fatigue)

CRACK PROPAGATION ON INTEGRATED RACEWAYS

Jörg Litzba
Joerg.Litzba@airbus.com
HoD Development drive-train components
Airbus Helicopters Technik GmbH
Calden, Germany

Waldemar Riesen
Waldemar.Riesen@airbus.com
Technology R&D Engineer
Airbus Helicopters Technik GmbH
Calden, Germany

Sven Hilleke
Sven.Hilleke@airbus.com
M. Structure Analysis Engineer
Airbus Helicopters Technik GmbH
Calden, Germany

Dr. Ramdane Boukellif
Ramdane.Boukellif@airbus.com
Technology R&D Engineer
Airbus Helicopters Technik GmbH
Calden, Germany

Abstract

Integrated raceways are often used within the design of helicopter main gearboxes aiming at a compact architecture with regards to a low overall gearbox weight. Due to the boundary conditions of using such raceways, a potential failure could have catastrophic consequences and it has to be ensured that all relevant failure modes are understood to ensure a safe and reliable operation. Rolling contact fatigue (RCF) and the related crack initiation and crack propagation plays a critical role in that context. Within an EASA initiated project fundamental research was conducted with the focus on RCF and crack propagation on integrated raceways. This paper will present the results from this research. As a first step, an analysis of key influencing parameters is performed, followed by a detailed description of the test campaign. Furthermore, the use of finite element analysis to predict crack propagation under RCF on integrated bearing raceways is studied, including the validation of simulation results through testing. Finally, a potential methodology for the implementation of the project results into the certification specification for helicopters CS27 and CS27 is presented.

1. NOTATION

Symbols:

MPa	Stress, N/mm²
Δa	Crack length extension, mm
GPa	Pressure, N/mm²
HV	Vickers Hardness, []
°	Angle, []
mm	Distance, mm
E	Young's modulus [MPa]
R	Radius, mm
μ	Friction coefficient, []
ν	Poisson's ratio, []
σ_1	Max. principal stress
ΔK_{th}	Stress intensity factor threshold, $N/mm^{3/2}$
ΔK_c	Critical stress intensity factor, $N/mm^{3/2}$
ΔK_v	Equivalent stress intensity factor, $N/mm^{3/2}$
ΔK_i	Stress intensity factor for Mode I, II or III, $N/mm^{3/2}$

Acronyms:

AHTech	Airbus Helicopters Technik GmbH
CRB	Cylindrical Roller Bearing

CS	Certification Specification
ERF	European Rotorcraft Forum
FE	Finite Element
FEA	Finite Element Analysis
FEM	Finite Element Modelling
MGB	Main Gearbox
MRO	Maintenance, Repair and Overhaul
MVCCI	Modified Virtual Crack Closure Integral
P.V.	Pressure Velocity
RCF	Rolling Contact Fatigue
SIF	Stress Intensity Factor
SRB	Spherical Roller Bearing

2. INTRODUCTION

Integrated raceways are often used within gearboxes aiming optimization of weight to power ratio and can be found on planetary gears or shafts made from case hardened material. Understanding of loading and failure modes is critical, to ensure reliable operation, since failures could lead to catastrophic accidents [1]. It is essential to understand the dependency between loading (rolling contact fatigue in combination with body stress due to optimized design parameters) and related failures modes (spalling with initial cracks followed by potential crack growth) to ensure the most robust design by avoiding mentioned failure modes. Furthermore, the designer needs a methodology, design criteria and numerical approaches for an efficient analysis during all design phases.

The paper is presenting the results of stream 2 of the EASA project “Integrity Improvement of Rotorcraft Main Gear Box (MGB)” under grant agreement number MOVE/B3/SUB/2020-243/SI2.826742.

3. OVERVIEW

The work that is described in this paper is focusing on fundamental understanding and potential prediction of crack propagation on integrated raceways under RCF, where the following separate work packages have been performed:

1. Analysis of available literature and field experience coming from relevant applications, incl. influencing parameters, state-of-the-art design methodologies and lessons learned from accidents
2. Test campaign using representative samples for helicopter MGB design (dimensioning, material, manufacturing, loads, etc). This includes the specification of test specimen, definition of test conditions and test benches as well as manufacturing of specimen and testing incl. in depth analysis of results
3. FE model definition and validation, that included the implementation of all relevant parameters into the FE model (e.g. residual stress condition, loading due to rolling contact and/or body stress, …) and simulation of crack propagation for various parameter settings. The FE model validation based on literature (e.g. observed cracks) and performed test campaign
4. Definition of recommendations for future design of MGB (influencing parameters, general method)

4. ANALYSIS

Due to the scope of the project that is described within this paper, the analysis is focused on integrated bearing raceways and very specific to the failure mode RCF (Rolling Contact Fatigue).

4.1. RCF – Definition of failure mode

Rolling contact fatigue (RCF) occurs when a surface is exposed to repeated rolling and sliding under high loads [2]. According to Ahmed [3], RCF can be defined as the mechanism of crack propagation caused by the near-surface alternating stress field within the rolling-contact bodies, which eventually leads to material removal. The formation of small craters in the surface (spalls) is referred to as spalling [2]. Additional types of damage related to RCF include subcase fatigue in surface hardened components (case crushing), surface originated pitting, peeling/micropitting and section fracture [4][5]. RCF can be found, for example, in ball and roller bearings, gears, cams, tappets and rails [3][6].

4.2. Determination of influencing parameters

The understanding of the failure mechanism of RCF is the key element in view of the definition of recommendations that will help the designer to avoid this failure mode for future design. To get this understanding three main sources of experience were investigated:

1. State-of-the-art design and verification process incl. relevant bearing concepts and key design parameters for bearings and particular parameters for integrated races
2. Principle contributing factors to crack initiation and propagation

3. Field experience from aviation, industrial and automotive application

Review of the state-of-the-art design and verification process showed, that a holistic approach incl. analytical (e.g. ISO/AGMA methods), numerical (FEA) or dedicated (company and application specific and advanced calculation methods) are usually applied and followed by verification using relevant testing procedures. Analysis further showed that the application of integrated races is usually limited to the bearing types SRB (Spherical Roller Bearing) and CRB (Cylindrical Roller Bearing).

Deeper analysis of these bearings showed that typical design parameters (“Key design parameters”) are used for aviation products, as shown in Table 1.

Parameter	Value
Tightening Hoop Stress	Case hardened steels around 250 MPa, through hardened steel max. 200 MPa
Contact stress	Below 1600 MPa in nominal condition Below 2200 – 2400 MPa in max. conditions
Misalignment	Misalignment until full contact / edge contact
Internal radial clearance	(0.015 – 0.22 mm) – should guarantee that with max. ring deformation loading angle zone is below 160 – 180°
Hardness	Surface hardness up to 850 HV (1100 HV for M50NiL nitrided)
Case hardening depth	Nitrided steels: 0.5 – 0.9 mm (HV_{Core}+100), Carburized steels: 0.3 – 1.6 mm at 550HV
Residual stress	Surface: -400 - -1000 MPa (for M50Nil nitrided: -1200 MPa) -

Table 1: Typical design parameter values (extract) [7]

In addition to the above shown design parameters, a fishbone analysis concerning contributing factors was performed. Due to the fact that not all identified design and contributing factors are impacting RCF with the same severity, an analysis concerning the criticality for reliability and flaw tolerance of bearing races was also done, identifying the parameters that are likely to have the most impact. These were highlighted with the criticality “high”:

- Contact stress
- Residual and body stress
- Misalignment
- Slippage and P.V.
- Lambda ratio lubrication
- Oil cleanliness / pollution
- Internal radial clearance and roller diameter
- Axial clearance and roller length
- Case pocket clearance
- Oscillation
- Material cleanliness and composition
- Hardness and Case hardening depth
- Residual and body stress
- Rim thickness
- Material and surface treatment
- Width of load zone

Furthermore, it can be concluded, that the design testing and selection of the correct parameters, isolated for each component, are well established processes, yet the interaction and impact of the parameters during operation remains largely uncontrolled and unresearched to date. It can be said that many of the mentioned parameters are influencing each other and cannot be optimized without having and influence on other parameters. For a better overview, the parameters with the classification “high” are shown in Figure 1.

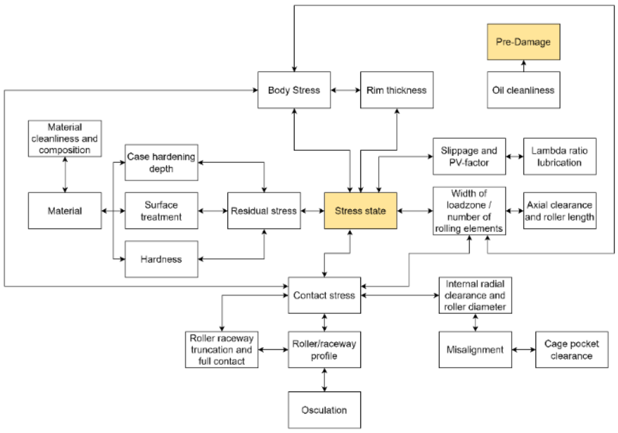

Figure 1: Interaction of critical parameters

For the most part, they all contribute similarly to the overall stress state of the integrated bearing races and therefore the potential of crack initiation. Oil cleanliness is a unique factor in this regard, as it does not directly contribute to the stress state, but does increases the risk of crack initiation due to particle overrolling and indentations on the raceway surface (pre-damage).

5. TESTING

5.1. Hypothesis

Based on analysis and detail literature research three (3) main hypothesis were defined:

1. In the case of a pure rolling contact load, an initiation of a crack with a finite depth may occur.
2. Without a complex load situation that is present for example in a planetary gear, there will be no further crack growth into depth under a single load of the rolling contact.
3. Only under the complex load situation (body stress), a crack propagation into the material is possible and has to be considered.

Test specimen are required in accordance with the three main hypotheses. For clear separation during the test campaign the test phases are named accordingly:

- Phase I.1 = Pure RCF for different load levels: The testing focused on the variation in contact pressure, whereas the other parameters were adjusted and fixed according to predefined baseline values.
- Phase I.2 = Pure RCF by varying key parameters: The focus for this phase was on the variation of hardness, residual stress, and hardening depth to evaluate their influence on crack initiation, depth, and shape.
- Phase II = RCF with additional body stress (complex load): This phase focused on the introduction of a complex load situation and the evaluation of its impact on crack propagation. All other parameters remained fixed according to the tested baseline variants from Phase I.1.

5.2. Specimens, Conditions and Benches

Therefore, test specimens (outer ring and shaft; both with two different materials) and the related test benches were identified, the type and method of testing to be performed were detailed, and the related inspection and acceptance criteria for verification were determined. Figure 2 shows the outer ring specimen with notch modification for phase II testing.

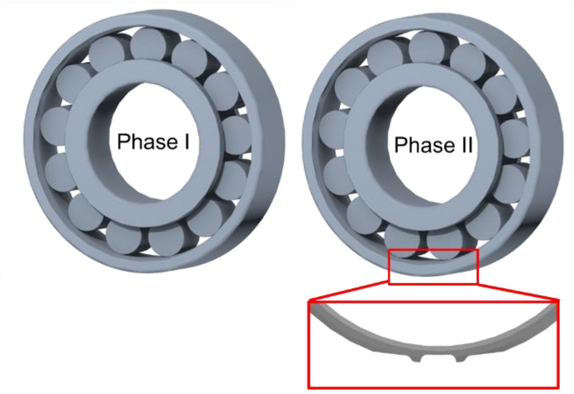

Figure 2: Outer ring specimen for phase I and II

The test bearing with the outer ring was mounted to test bench with two support bearings (see Figure 3).

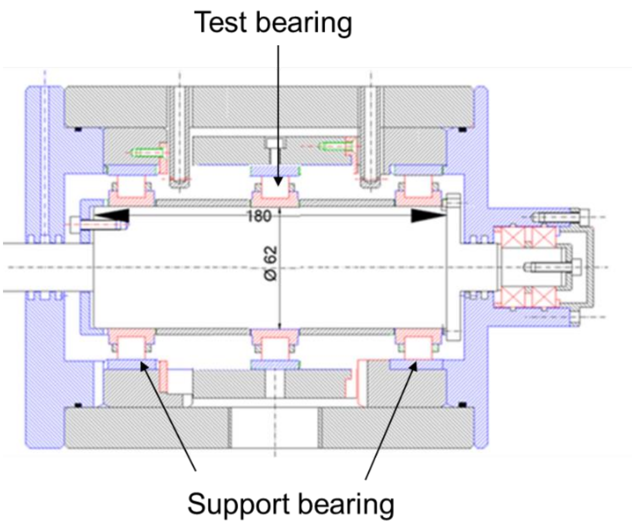

Figure 3: Test bench for outer ring specimen

The shaft specimen with modification for phase II testing is shown in Figure 4.

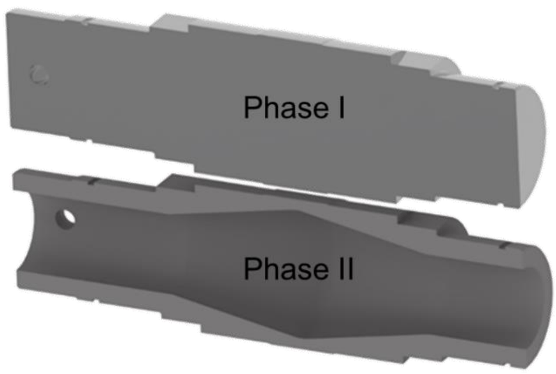

Figure 4: Shaft specimen for Phase I and II

The shaft specimen was mounted to the test bench (see Figure 5) by three support bearings, whereas the bearing in the middle was used to introduce the radial load and rolling contact.

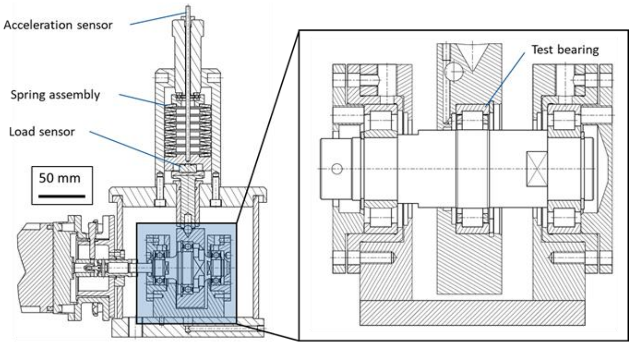

Figure 5: Test bench for shaft specimen

A list of the main test parameters for both test benches is highlighted in Table 2.

Parameter	Outer ring bench	Shaft bench
Speed max. [rpm]	8000	6000
Oil temp. [°C]	70-80	
Oil type	AirGo 3001	
Lubrication property	λ>2	κ>1.7
Load level [MPa]	1500-2400	

Table 2: Test conditions

The purpose of the outer ring specimen was to evaluate the integrated outer races. To introduce the complex load situation, the design of the specimen was modified with a notch/groove in the outer ring to enable the outer ring to bend under the roller load.

The purpose of the shaft specimen was to evaluate integrated inner races. To introduce the complex load situation on this specimen, the solid shaft specimen was replaced by a hollow shaft to enable the application of radial force and therefore a bending load and bending stress on the shaft. Table 3 and Table 4 give an overview of the different variants, which were tested for the two types of specimen. For each variant 3 samples were foreseen for testing.

Variant	Material	Manufacturing approach	Test phase
1	16NCD13	Basic variant	I.1
1.1	16NCD13	Basic variant (hollow)	II
2	32CDV13	Basic variant	I.1
2.1	32CDV13	Basic variant (hollow)	II
3	16NCD13	Adjusted heat treatment	I.2
4	32CDV13	Adjusted heat treatment	I.2
5	16NCD13	Adjusted heat treatment	I.2
6	32CDV13	Adjusted heat treatment	I.2
10.1	32CDV13	Adjusted heat treatment	I.2
11	16NCD13	Intermediate heating and surface finish adjustment	I.2

Table 3: Overview of variants for shaft specimen

Variant	Material	Manufacturing approach	Test phase
B	M50Nil	Basic variant	I.1
DA	32CDV13	Basic variant	I.1
BB	M50Nil	Adjusted heat treatment	I.2
DC	32CDV13	Adjusted heat treatment	I.2
BA	M50Nil	Adjusted heat treatment	I.2
DB	32CDV13	Adjusted heat treatment	I.2
BC	M50Nil	Adjusted surface finish process	I.2
DD	32CDV13	Adjusted surface finish process	I.2
T102	M50Nil	Basic variant – Notch severe design	II
T102	32CDV13	Basic variant – Notch severe design	II
T104	M50Nil	Basic variant – Notch less severe design	II
T104	32CDV13	Basic variant – Notch less severe design	II

Table 4: Overview of variants for outer ring specimen

5.3. Results

Phase I.1 was used to study the influence of different load levels on the initiation of spalling and cracks under pure RCF for a pre-damaged raceway. The results demonstrated that a limit exists for both materials, below which no spalling could be introduced for the given pre-damage, whereas the load level of 2.4 GPa repeatably produced spalling.

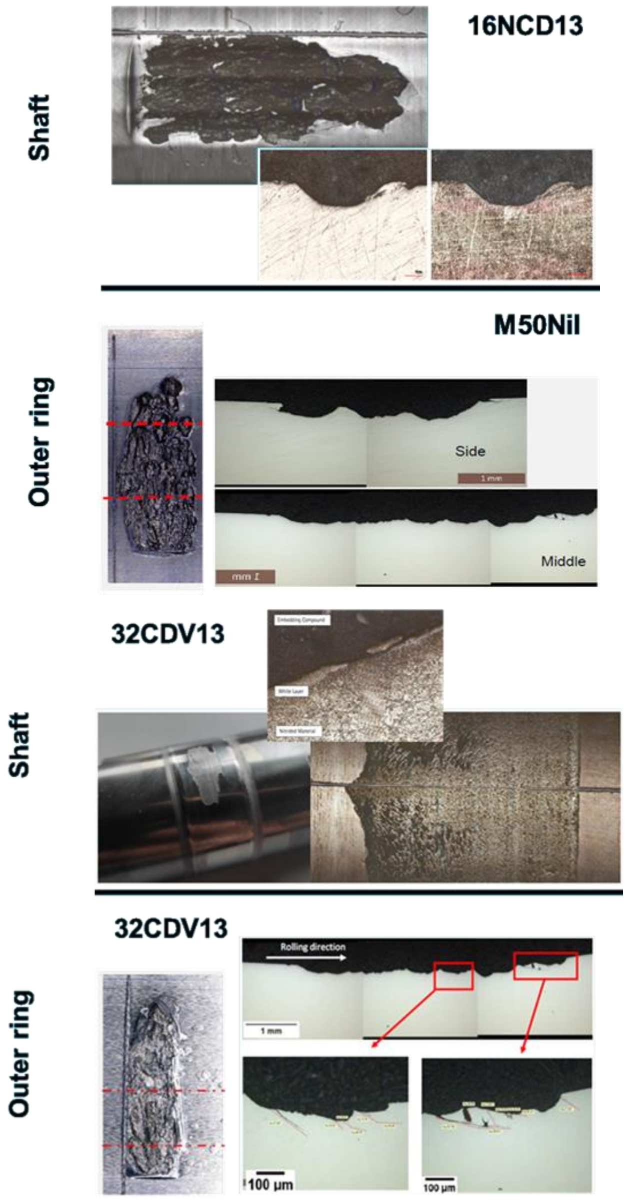

Figure 6: Typical spalling at ≥ 2.4 GPa;
no crack propagation into depth [12]

Identical observations were made for Phase I.2, where parameters such as hardness depth, hardness, and residual stress were varied. Within the three load levels that were tested, the limit for no spall initiation remained below 2.4 GPa, initiation of spalling was only possible at a load level of 2.4 GPa A more detailed limit could not be identified because only three load levels were tested. Nevertheless, a clear trend was not observed for both materials and applications; however, by variation of case hardening depth, it was observed that specimens with highest case hardening depth led to lowest spalling depth, as long as only heat treatment process is changed compared to baseline variants V1 and B (see Figure 7 and Figure 9). For V11, not only heat treatment adjustments were implemented, but also additional surface rolling. Finally, all the tests for Phase I.1 and I.2 validated the hypothesis that crack growth ends at a finite depth and pure rolling contact typically results in classical spalling damage for the single load condition without further crack growth through the material. For completeness Figure 7 to Figure 10 give an overview of the measured spalling depth after testing.

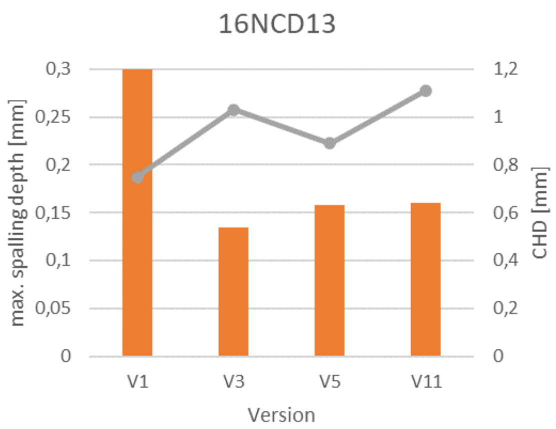

Figure 7: Shaft application:
Max. detected spalling depth (16NCD13) [12]

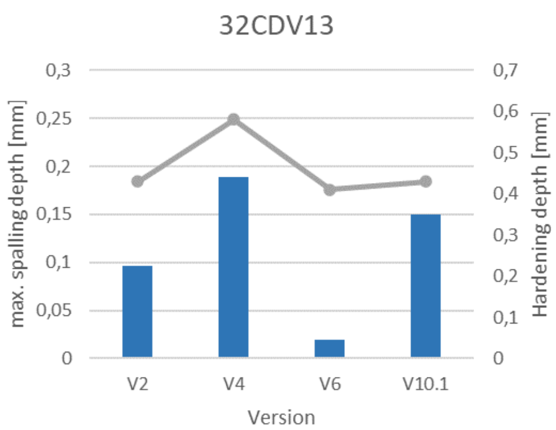

Figure 8: Shaft application:
Peeling of white layer (32CVD13) [12]

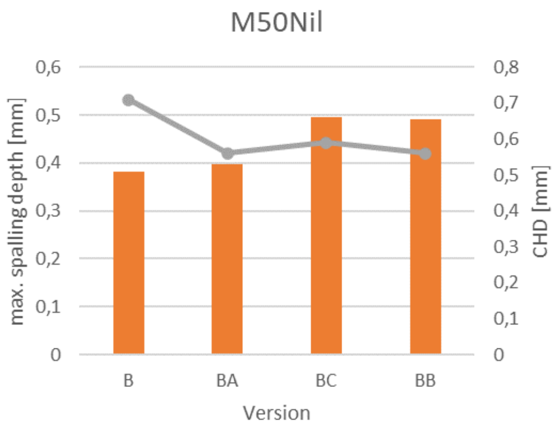

Figure 9: Outer ring application:
Max. detected spalling depth (16NCD13) [12]

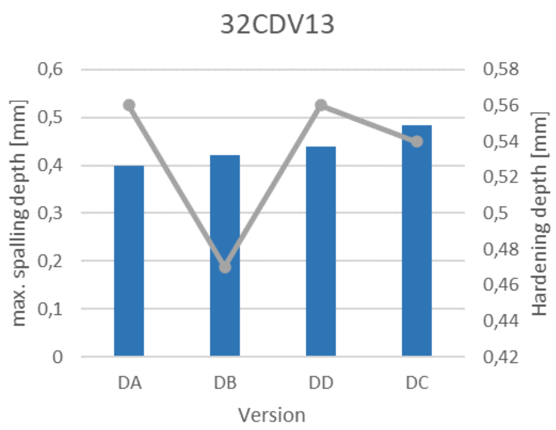

Figure 10: Outer ring application:
Max. detected spalling depth (32CVD13) [12]

The results for shaft application from 32CDV13, are only of limited significance, as they did not show any classic spalling. The reason for this is that the white layer is not removed for the nitrided shafts during the manufacturing process and led to a peeling-off of the white layer.

During Phase II, a complex load was introduced by modification of the specimens, thereby allowing additional deformations. The tests showed for the outer ring application that the body stress led to severe cracks into the depth of and through the material. It was also shown that for the same load level, no cracks through the material occurred for the nitrided material, which could be explained by a higher crack growth threshold value. For the shaft application, it was only possible at a much higher load level (2.9 GPa) to introduce further crack growth Nevertheless, it was not possible to reach a cracking into depth of the part for the shaft samples with the initial damage. This required a larger pre-damage as shown in Figure 11 and Figure 12. Cracks perpendicular to the raceway were observed to be less critical to the bending moment because only the ovalization of the shaft promotes crack propagation as an additional driver. As this is only a hypothesis, further testing with cracks in the rolling direction and larger pre-damage should be carried out to prove this hypothesis.

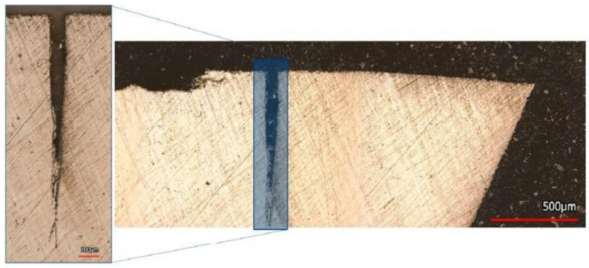

Figure 11: 16NCD13 shaft at 2.9 GPa
with laser scratch [12]

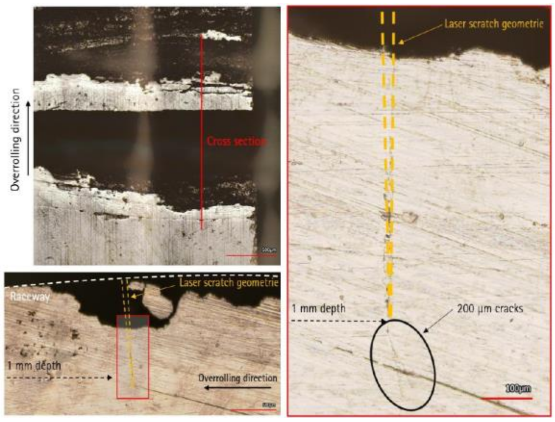

Figure 12: 32CDV13 shaft at 2.9 GPa
with laser scratch [12]

The results for the outer ring application are presented in Figure 13 and Figure 14. With additional body stress, it was possible to reach a crack through the component for M50 Nil material, whereas no cracks were observed for the nitrided variant.

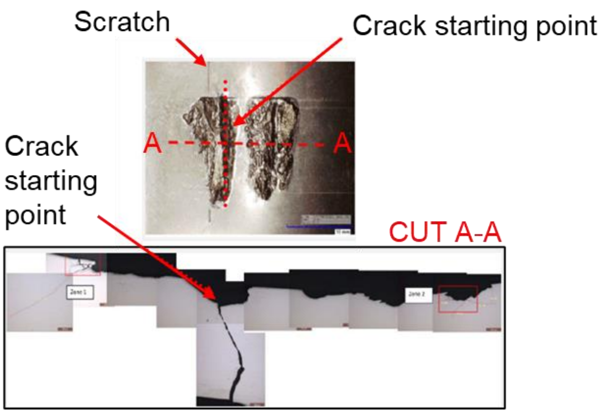

Figure 13: M50Nil outer ring at 2.4 GPa [12]

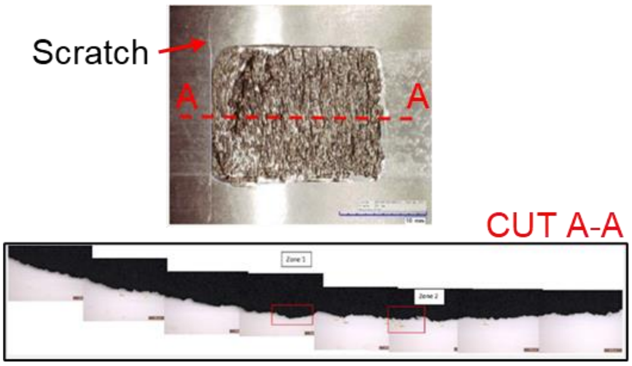

Figure 14: 32CDV13 outer ring at 2.4 GPa [12]

Nevertheless, the test results showed that deeper crack propagation into the depth of the material with a crack through the complete thickness is mainly driven by the additional body stress, and the potential for this type of failure can be significantly reduced by the reduction or omission of body stress.

6. SIMULATION USING FEA

The crack growth simulation is carried out using stress intensity factor approach, with the program system ADAPCRACK3D. Using FEM, the domain around the growing crack is replaced by a sub-model. The program system ADAPCRACK3D consists of three programs [8]. With the first sub-program NETADAPT3D, all mesh adjustments resulting from the propagating crack are carried out. In the second part, ABAQUS solves a FE- calculation for each iteration step. This provides the displacements and forces, stresses and strains for all nodes. From the nodal forces and nodal displacements, the third module NETCRACK3D calculates the SIFs ΔK_i $(i = I, II,\ III)$ along the crack front using MVCCI [9]. Using the σ_1' criterion [10], the cyclic equivalent SIF ΔK_V as well as the kink angles are determined. If ΔK_V is smaller than the threshold value, the crack cannot grow. If the crack propagation is subcritical ($\Delta K_{th} < \Delta K_V < \Delta K_C$), the crack is extended by Δa, taking into account the kink angle. The crack growth simulation is continued until the fracture toughness. In this cases, linear-elastic fracture mechanics and an initial technical surface crack is assumed for the fracture mechanical investigation. Due to the large number of interactively influencing parameters, such as contact geometry, load, lubricating film, rolling velocity, coefficient of friction, material properties, surface treatment, impurities, etc. [11], rolling contact fatigue is a complex problem. To get a more accurate correlation with tests, following important parameters are considered: contact geometry, loading friction at cylinder/half-plane and at crack flanks and residual stress profile. The mechanical properties of the materials used are similar.

6.1. Parametric study to prepare Phase I.1

A parametric study was conducted in advance to prepare Phase I.1 testing. The crack paths were investigated assuming a semi-infinite plane with an edge crack under pure rolling contact load by varying the following parameters: initial crack length, crack angle, friction coefficient, contact pressure and friction coefficient at the crack surfaces. The equivalent stress intensity factor ΔK_V for the growing crack is compared with the typical threshold value of approx. 150 $N/mm^{3/2}$ against fatigue crack growth in steel. This limit is represented by red line in the figures (see Figure 16). As an example, a case from the parameter study was selected and compared with the test results. Further results of the parameter study can be found in [12]. The parameters used for the simulation are given in Table 5.

Parameters used in the simulations	
Initial crack length	0.5 mm
Crack angle	15°
Friction coefficient cylinder/half-plane	0.15
Contact pressure	1500 N/mm^2
Friction coefficient crack surfaces	0.15
Residual stress	No
Material properties	
Young's modulus E [MPa]	211000
Poisson's ratio ν	0.3

Table 5: Parameters used for the simulation in Figure 15

Figure 15 describes the crack paths of the crack growth simulation with the test in Phase I.1. under pure rolling contact with the parameters defined in Table 5.

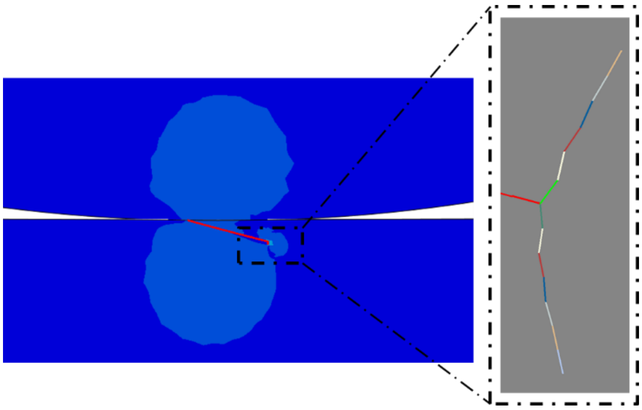

Figure 15: Simulation results phase I.1

We could observe in Figure 15 and Figure 16 that after crack branching, the lower crack stops earlier than the upper crack. It was predicted that crack propagation would only occur to a limited depth into the material. The upper crack grows slowly towards the surface (possibly no crack stopping). In the test, spalling was observed and no crack growth into the depth of the material. The test results correlate well with the results in the simulation.

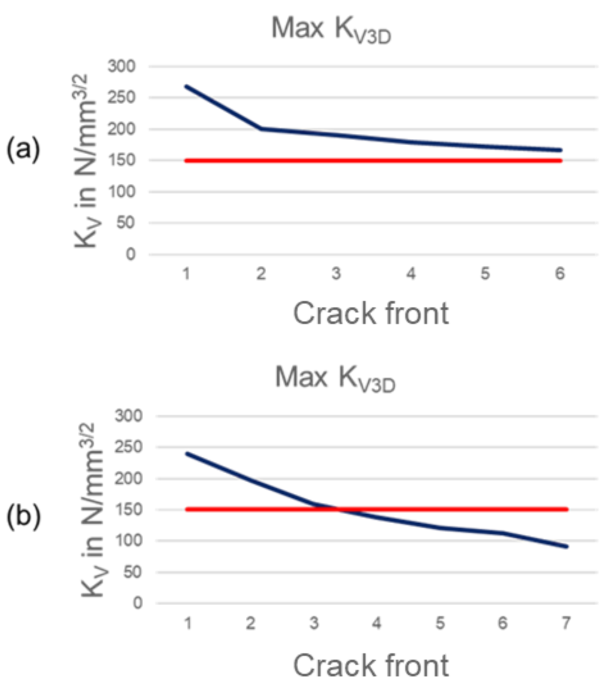

Figure 16: Max K_V during crack growth in Figure 2; (a) for the upper crack path. (b) for the lower crack path [12]

6.2. Phase I.2

In preparation for Phase I.2, a parameter study was carried out to investigate the influence of residual stresses and pure rolling contact on crack growth. The aim of Phase I.2 was to investigate the maximum crack growth depth and the tendency of crack propagation (into the core or back to the surface) in comparison to the base variant of Phase I.1.

The residual stresses were modelled using thermal stresses, as shown in Figure 17. The temperature that results in thermal expansion is specified in the model. By limiting the expansion, e.g. by means of fixed clamps, thermal stresses are generated that correspond to the residual stresses. The relevant thermal expansion coefficients are determined by control calculations and thus also by the distribution of the residual stresses. The approximated residual stress curve used in the simulation are based on the measured residual stresses of planetary gears from the ZF Group (see Figure 18). Measurements were also taken for the shaft and outer ring specimens and the simulations were adapted accordingly.

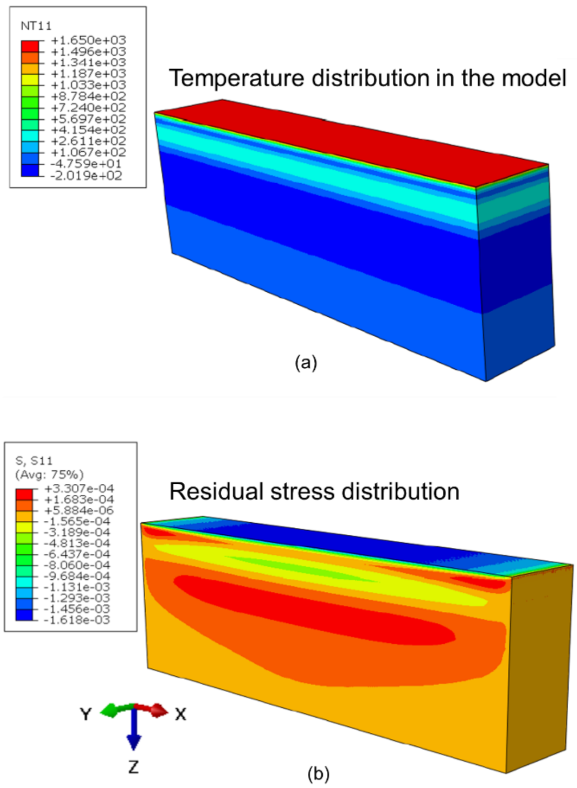

Figure 17: Modeling of residual stresses due to thermal stresses, (a) temperature distribution in the model, (b) residual stresses [12]

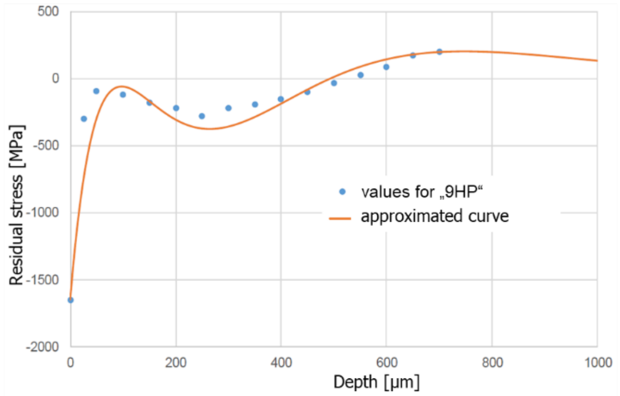

Figure 18: Approximate residual stress curve used for FE-analysis [12]

The crack growth simulation was performed for the case described in Table 6 and stopped shortly before complete crack propagation to the surface ("complete spalling"), so that a meaningful evaluation could take place, see Figure 21. The crack growth after kinking occurred almost under Mode I loading. Near the edge, the crack extension is almost perpendicular to the surface. In this case, spalling is expected.

Parameters used in the simulations	
Initial crack length	0.5 mm
Crack angle	15°
Friction coefficient cylinder/half-plane	0.15
Contact pressure	1500 N/mm²
Friction coefficient crack surfaces	0.15
Residual stress	yes
Material properties	
Young's modulus E [MPa]	211000
Poisson's ratio ν	0.3

Table 6: Parameters used for the simulation

The crack after kinking was mainly growing under Mode I loading. K_I without residual stresses were calculated and compared with those of the current case (with residual stresses) (see Figure 19). Although the two crack paths are similar up to front 6 (see Figure 20), the two graphs of the K_I differ. The residual stresses increase the K_I values significantly. While the non-residual stress crack stops (K_I decreases, near K_{th} =150 N/mm$^{3/2}$), the crack with residual stress is able to grow (K_I is constant and much larger than K_{th}). That means the crack without residual stresses may propagate deeper or back to the surface, while the crack with residual stresses will only return to the surface.

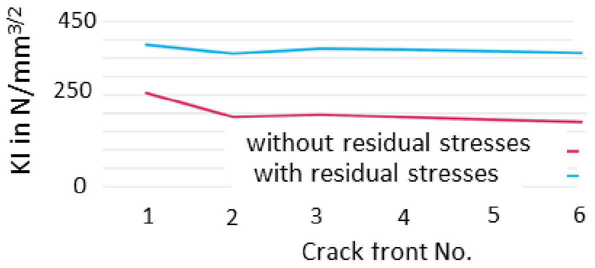

Figure 19: Influence of residual stresses on the KI graph after kinking under rolling contact [12]

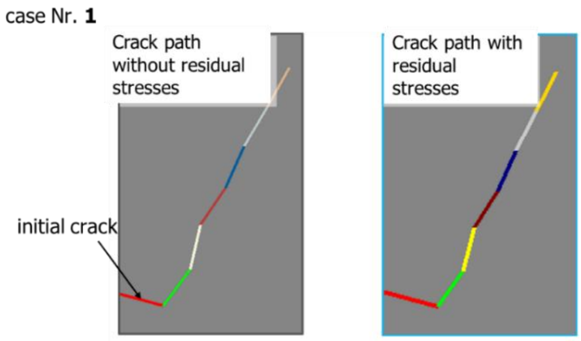

Figure 20: Comparison of the crack paths with and without residual stresses under rolling contact [12]

Figure 21 shows the comparison between the crack growth simulation and the results of the outer ring test. In the simulation, it is clearly seen that the crack grows towards the surface and spalling is to be expected (see Figure 21, above). In the test, spalling was observed and not a continuous crack. The crack propagation only occurred to a limited depth (see Figure 21, below).

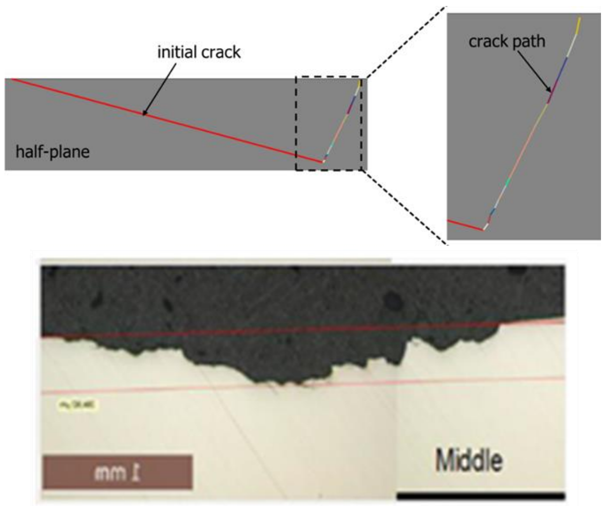

Figure 21: Results phase I.2: Comparison simulation (above) and testing (below) [12]

6.3. Phase II

In phase II the influence of an additional load (complex load) was investigated. Using the measured residual stresses, crack growth simulations were carried out in the hollow shaft and in the outer ring. The results of the crack growth simulations showed good agreement with some results of the tests.

6.3.1. Hollow shaft

For the simulation of fatigue crack growth under rolling contact in the hollow shaft, the parameters in Table 7 are considered.

Parameters used in the simulations	
Friction coefficient (cylinder/hollow shaft - no slipping)	0.15
Friction coefficient (crack surfaces)	0.15
Cylinder radius R [mm]	9
Maximum contact pressure p_0 [MPa]	2400
Inside radius [mm]	32
Outside radius [mm]	37.5

Material properties/32CDV13	
Young's modulus E [MPa]	211000
Poisson's ratio ν	0.3

Table 7: Definition of the parameters and material properties used in the crack growth simulation in the hollow shaft under rolling contact fatigue

The predicted crack path and the crack growth in the test of V2.1/4 are shown in Figure 22. The crack in the simulation grew straight from the notch in the radial direction without crack branching, as shown Figure 22 (a). A comparable crack propagation from 1 mm, as indicated by the red line (starting from the laser scratch) can be observed in Figure 22 (b), whereby a crack network also formed during the test and the presence of any crack propagation in to the depth from the bottom of laser scratch, as indicated by the red line, is questionable. It was predicted by the simulation that the crack would continue to grow due to high tensile residual stresses until total failure of the hollow shaft. The cracks only grew slightly deeper in the real tests. The resulting crack networks on the surface next to the notch were probably due to the influence of the white layer. This assumption requires further study [12].

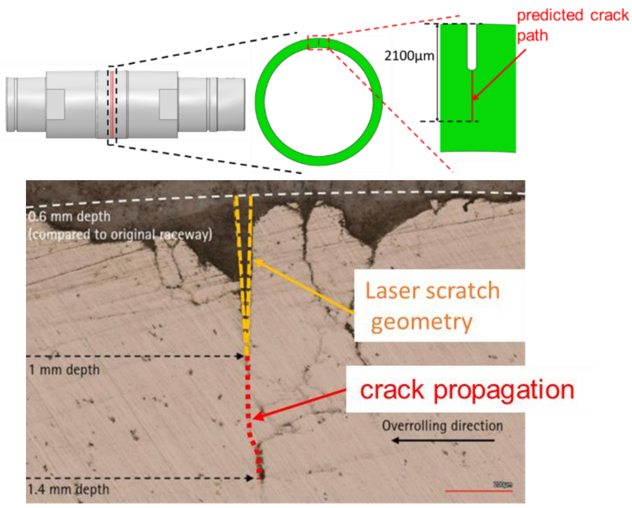

Figure 22: Comparison between the numerical and real tests, (a) prediction of the crack path under RCF considering the residual stresses in the hollow shaft, (b) crack propagation from 1 to 1.4 mm starting from the laser scratch and crack network near the surface and the scratch of shaft V2.1/4 [12]

6.3.2. Outer ring with notch

The crack growth simulations in the outer ring with the notch design T104 were carried out taking into account the parameters given in Table 8.

Parameters used in the simulation	
Friction coefficient (cylinder/outer ring - no slipping)	0.15
Friction coefficient (crack surfaces)	0.15
Cylinder radius R [mm]	11.97
Maximum contact pressure p_0 [MPa]	2400

Material properties/M50NiL	
Young's modulus E [MPa]	205000
Poisson's ratio ν	0.3

Table 8: Definition of the used parameters and material properties used in the crack growth simulation in the outer ring under rolling contact fatigue

In general, the predicted crack paths showed good agreement with only some tests. The calculated crack path with an initial crack length of 1.5 mm was compared with the resulting crack in the outer ring made of M50Nil, T104/SN221025. The predicted crack path agrees very well with the crack path in the real test, using 3 samples, see Figure 23. To determine the direction of further crack growth in part II, the maximum principal stresses are evaluated (see Figure 23). This shows that there is a high base loading in the remaining cross-section. This loading situation can lead to the complete fracture of the remaining cross-section due to strength failure. In this case, sharp kinking of the crack is very likely. The quantitatively expected direction of further crack growth in area II is shown Figure 23. In the test with the material 32CDV13, no crack growth into depth could be generated.

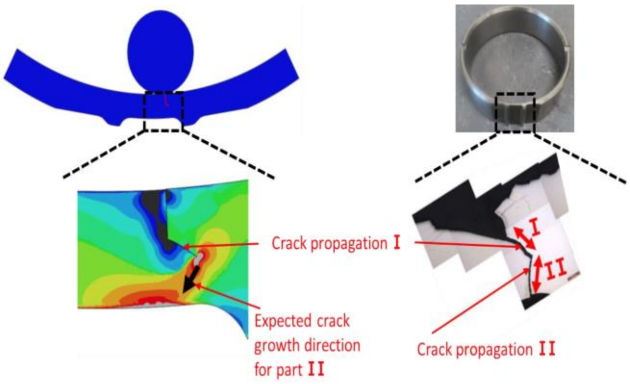

Figure 23: Schematic representation of the comparison between crack propagation in the test and the crack growth simulation, (a) crack path prediction by the crack growth simulation, (b) crack propagation during the test of "M50Nil Version 1 T104 S/N221025"

7. METHODOLOGY FOR RCF ASSESSMENT

Based on the content of GIFT research project a methodology for RCF component assessment was established. The methodology aims to provide support for verification of CS27/29.571 paragraph for integrated bearing races with catastrophic failure mode. The approach is based on four main steps and is visualized in Figure 24.

1. Evaluation of component design values
2. Collection of additional MRO data and use of experience from GIFT project
3. Setup of FE simulation and provisions of recommendations for redesign
4. Validation by testing

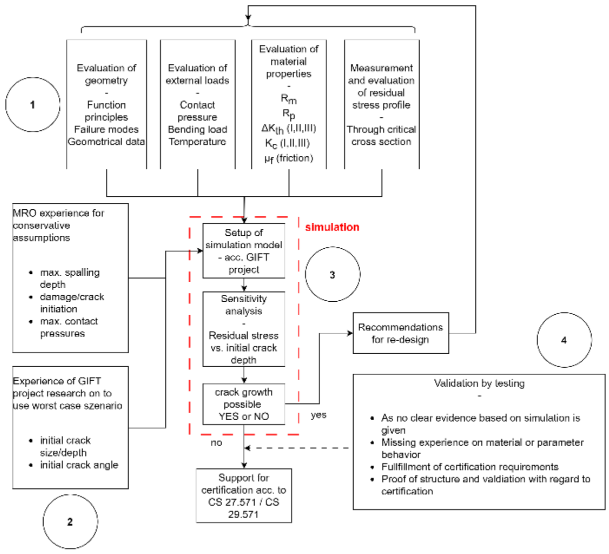

Figure 24: Methodology for RCF component assessment based on GIFT project

8. CONCLUSIONS

1. Damage mechanism and failure modes of bearings using integrated raceways were analyzed. Results were used for definition of representative test specimen, test conditions and test benches. A test campaign was performed, analyzing the impact of design and manufacturing parameters on the development of RCF followed by crack initiation and crack propagation.

2. The defined main hypotheses concerning RCF and development of crack propagation were confirmed.

3. Based on in depth analysis, a FE model for crack propagation was developed and validated within the project scope. Validation was performed using data from literature and the results of the test campaign of this project. The simulation was limited to 2D and based on some simplifications to improve calculation time (e.g. sub-modelling, material definitions, 2D vs. 3D stress field), but could be extended to 3D and more model complexity if required. Although the test results matched the simulation results in general well, the simulations for the specimen with body stress showed some discrepancies with the test results. Further investigations are necessary for root cause analysis.

4. A methodology was developed that allows the designer in an early stage to evaluate a potential risk for crack growth on integrated raceways. Due

to the nature of the discussed failure mode, each single design has to be analyzed separately. The methodology will contribute to CS27/29.571 and may include test procedures that have been developed during this project to evaluate a potential risk for crack growth on integrated raceways under RCF. Nevertheless, the presented methodology requires testing on the component under investigation, in order to validate simulation approach for other applications.

5. Follow on research is recommended to extend the knowledge gained during this project, since some technical aspects could not be discussed and analyzed in the recommended depth within the defined project scope. Additional work should also include further testing for statistical reasons.
6. Some topics could not be covered in detail within the test campaign and could be a basis for further testing. This includes the validation of test results for different initial damages, an extended range of material properties and additional intermediate test points (e.g. for contact pressure, residual stress and body stress). Further studies could also be done on maximum crack depth and confirmation with simulation.

9. ACKNOWLEDGMENTS

The authors would like to acknowledge the support of the involved team at EASA and the project partners SKF Aerospace, IMKT from University of Hannover, University of Paderborn, Central R&D of ZF AG and all colleagues at Airbus Helicopters Technik that participated during the time of the project.

10. REFERENCES

[1] Accident Investigation Board Norway (AIBN), report 'Report on the Air Accident near Turøy, Øygarden, Municipality, Hordaland Country, Norway 29 April 2016 with Airbus Helicopters EC 225 LP, LN-OJF, Operated by CHC Helikopter Service AS', SL 2018/04, July 2018

[2] Department of Solid Mechanics, Royal Institute of Technology, study 'A Study on Contact Fatigue', 2000.

[3] R. Ahmed, book chapter 'Rolling Contact Fatigue', ASM Handbook, Vol. 11, Failure Analysis and Prevention, 2002.

[4] A. V. Olver, book chapter 'The Mechanism of Rolling Contact Fatigue: an Update', Proc. IMechE Vol. 2019 Part J, 2005.

[5] NASA, report 'The Mechanism of Contact Fatigue', NASA Special Report SP-237, 1969/1970.

[6] ASM International, handbook 'Contact Fatigue', ASM Handbook, Volume 19: Fatigue and Fracture, 1996.

[7] S. Hilleke and W. Riesen, Integrity improvement of rotorcraft main gearbox (EASA.2019.C15), 'D2-1: Determine design parameter (2021) '

[8] M. Fulland, M. Schöllmann, H. A. Richard. ADAPCRACK3D - Development of the program for the simulation of three-dimensional crack propagation processes. In: S.N. Atluri, F.W. Brust (Eds.): Advances in Computional Engineering & Sciences, Vol. I, Tech Science Press, Palmdale, USA (2000), 948-953

[9] E.F. Rybicki and M.F. Kanninen, "A finite element calculation of stress intensity factors by a modified crack closure integral", Engineering Fracture Mechanics, 9 (1977), 931-938

[10] M. Schöllmann, H.A. Richard, G. Kullmer et al., "A new criterion for the prediction of crack development in multiaxially loaded structures", International Journal of Fracture 117 (2002), 129-141

[11] D. Hannes, On fatigue crack growth modelling of surface initiated rolling contact fatigue using the asperity point load mechanism, Doctoral Thesis no. 85, Department of Solid Mechanics, School of Engineering Sciences KTH Royal Institute of Technology, Stockholm, Sweden (2014)

[12] R. Boukellif, S. Hilleke and W. Riesen, Integrity improvement of rotorcraft main gearbox (EASA.2019.C15), 'D2-7: Test report and conclusions (2024)'